Parametric Model for Compensation of Partial Volume Effect in CT Iterative Reconstruction

Jean-Baptiste Thibault, *Member, IEEE*, Kai Zeng, Lin Fu, Zhou Yu, *Member, IEEE*, Thomas Benson, Bruno De Man, *Member, IEEE*, Ken Sauer, *Member, IEEE*, and Charles Bouman, *Fellow, IEEE*,

***Abstract*—Iterative reconstruction methods relying on linearization of the relationship between images and projections have to cope with the inherent representation of the scanned object by voxel elements. When the voxel size becomes large enough to reduce the overall computational requirements, partial volume can become an issue for overall image quality. We propose in this paper a linear parametric model with the purpose of providing a better representation of the object in regions of rapid variations in local density. We show that this approach is effective at retaining the quality of thin slice reconstructions without explicitly modeling thinner slices. Good image quality is obtained at a significantly reduced computation cost relative to that of using finer sampling of the image volume.**

***Index Terms*—Computed tomography, iterative reconstruction, parametric model, linear partial volume.**

I. Introduction

With its recent introduction into CT clinical practice, Model-Based Iterative Reconstruction (MBIR) has been shown to be effective at improving image quality performance in both low-dose and high resolution applications [1], [2]. One of the advantages of this framework is that it supports using accurate system models to describe the interaction between image volume and projection space in a manner representative of the real system. The spatially-varying nature of the forward model can be taken into account to optimize spatial resolution while correctly handling the cone-beam geometry and improving overall statistics by considering large sets of connected projection components in the log-likelihood. However, the standard linearized model with

$$\mathbf{y} = \mathbf{A}\mathbf{x} + \mathbf{n}, \tag{1}$$

where $\mathbf{y}$ represents the projection data, $\mathbf{x}$ the unknown image volume, and $\mathbf{n}$ an additive noise vector, implies a discretization that often leads to rectangular voxels or "blob" models [3]. Although classical Nyquist theory points to using voxel sizes equivalent to half the detector sampling [1], modern scanner technology would require voxel sizes so small that such models would become computationally impractical. But the piecewise constant nature of the rectangular image model can create difficulties in situations where the continuous object contains strong gradients of density. For example, high resolution reconstructions with high in-plane resolution but low cross-plane resolution may suffer from image artifacts, such as the artificial enhancement of bone boundaries and underestimation of surrounding soft tissue density in regions of large local z-gradients in Figure 1. Such issues are greatly reduced by reconstructing the same volume over a finer grid. This illustrates the sensitivity of standard voxel-based forward modeling to linear partial volume effects.

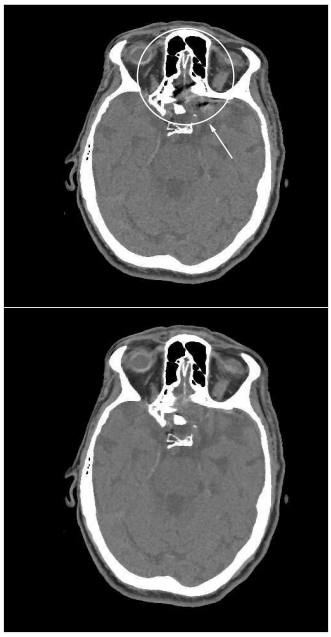

Fig. 1. Iterative reconstruction of a patient's head from a 32x0.625mm axial scan. The top image is reconstructed at 0.625mm thickness; the bottom image at 0.3125mm. Low frequency shading artifacts appear in the thick slice image around the sinus area which includes strong z-gradients.

In this paper, we present a new parametric approach to further improve the system model in MBIR by allowing piecewise linear rather than piecewise constant modeling of the reconstructed volume to better represent regions of large gradient in the scanned object. This approach can provide improved object representation and is more computationally efficient than simply using a smaller reconstruction grid.

Jean-Baptiste Thibault and Zhou Yu are with the CT Systems and Advanced Algorithms group, GE Healthcare, Waukesha, WI 53188, USA;
Thomas Benson, Bruno De Man, Lin Fu, and Kai Zeng are with the CT Systems and Applications Laboratory, GE Global Research, Niskayuna, NY 12309, USA;
Ken Sauer is with the Department of Electrical Engineering, University of Notre Dame, Notre Dame, IN 46556, USA;
Charles Bouman is with the Department of Electrical and Computer Engineering, Purdue University, West Lafayette, IN 47907, USA;

II. Parametric Formulation

A. Piecewise Linear Forward Model

Standard image reconstruction considers individual voxels as constant valued. To better represent rapid variations in density in a quantized framework, we propose a simple linear model for possible changes of density within each voxel, where each element of $\mathbf{x}$ becomes a two-dimensional vector representing continuous variation of the density of a voxel

$$x_j(t) = \alpha_j + \beta_j \times (t - 0.5), \tag{2}$$

where α_j and β_j are the DC and slope components of voxel j, respectively, and t is a parameter representing displacement along the length of the voxel. In this parametric model, the reconstructed volume is piecewise linear instead of piecewise constant. Equation (1) becomes

$$\mathbf{y} = \mathbf{A}\alpha + \mathbf{B}\beta + \mathbf{n},$$

where $\mathbf{A} = \{a_{ij}\}$ and $\mathbf{B} = \{b_{ij}\}$ are the respective components of the forward model for either of the DC and slope voxel coefficients.

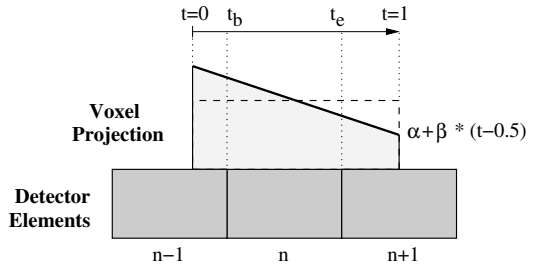

Fig. 2. Illustration of the calculation of the coefficients of the piecewise linear forward model in a distance-driven framework. Compared to the conventional model with constant voxel (dashed line), the value of the voxel is allowed to change linearly over the length of its projection profile onto the detector (bold line). α now represents the value of the voxel at its center point, and β is the slope of the allowed variation along the considered dimension.

In one dimension, using the Distance-Driven (DD) formulation [4], the coefficients of the forward model can be computed as illustrated in Figure 2. The DD model represents the convolution of the finite voxel and detector responses. Figure 2 shows the profile of the projection of the voxel onto the detector axis. Instead of the constant value in the dashed line, the sloped linear model of (2) allows the density of the voxel to change along the considered dimension, parameterized by $t \in [0, 1]$ over the face of the projection of the voxel onto the detector axis. Let t_b and t_e be the values of t at the beginning and end detector boundaries over that range. The coefficients associated with each detector value are then:

$$\begin{aligned} a_{ij} &= t_e - t_b \\ b_{ij} &= \frac{(t_e + t_b - 1)}{2}(t_e - t_b). \end{aligned}$$

B. Modified Cost Function

Under this linear parametric model, the cost function of the maximum *a posteriori* (MAP) estimation problem, with the usual quadratic approximation to the log-likelihood, is written as:

$$\left\{\hat{\alpha}, \hat{\beta}\right\} = \arg\min_{\alpha,\beta} \left\{ \frac{1}{2}||\mathbf{y} - \mathbf{A}\alpha - \mathbf{B}\beta||^2_{\mathbf{W}} + U(\alpha, \beta) \right\}. \tag{3}$$

Here, $\mathbf{W}$ is a statistical weighting matrix with entries approximately inversely proportional to the variance in the raw measurements, and $U(\cdot, \cdot)$ is a (possibly joint) regularization function for each of the voxel components.

With twice as many image coefficients to compute as in the standard piecewise constant model, proper regularization is important to stabilize the estimation process. We consider here simple independent spatial regularization of α and β using standard regularization framework developed for MBIR, with the advantage of retaining the strict convexity of the overall cost function for reliable convergence and the associated frequency characteristics designed for the resulting image. We have found the q-Generalized Gaussian MRF (q-GGMRF) [1], noted here $U_q(\cdot)$ to provide both appropriate low-intensity smoothing as well as edge preservation, and propose

$$U(\alpha, \beta) = U_q(\alpha) + U_q(\beta). \tag{4}$$

We note that the nature of the slope coefficient pushes it near zero in relatively homogeneous regions occurring with high probability in medical imaging applications. This indicates that L_1 regularization of β may prove beneficial, which we leave for further research at this time.

C. Computation of the Solution

Our overall optimization approach follows the sequential pattern used in iterative coordinate descent (ICD), with the normal image vector augmented to contain both the DC and slope components in $\mathbf{x} = [\alpha, \beta]^T$. ICD has demonstrated satisfactory convergence in many reconstruction problems in fewer than 10 iterations when initiated with the FBP reconstruction. To further optimize convergence, we use spatially non-homogeneous ICD (NH-ICD), which focuses computation where it is most needed according to the history of voxel updates [5].

The ICD algorithm decomposes the global optimization problem into a sequence of greedy one-dimensional update calculations for each voxel x_j while keeping all others in a fixed state. In the case of the two-valued model for the piecewise linear approach, however, this turns into the joint optimization of α_j and β_j for each voxel, as

$$\left\{\hat{\alpha}_j, \hat{\beta}_j\right\} = \arg\min_{\alpha_j,\beta_j} \left\{ \frac{1}{2} \sum_i w_i \left(y_i - a_{ij}\alpha_j - b_{ij}\beta_j - C_{i,j}\right)^2 + U(\alpha_j, \beta_j) \right\}, \tag{5}$$

where $C_{i,j}$ is a constant for voxel j dependent on the projection of the full image volume except for x_j. The solution of this parametric estimation problem follows from the framework originally developed in [6] for PET kinetic parameter reconstruction.

Let's turn our attention to the log-likelihood term in equation (5). The quadratic nature of this function leads to an equation of the form:

$$\frac{1}{2}x_j^T\mathbf{Q}x_j + \mathbf{b}^T x_j \tag{6}$$

where

$$\mathbf{Q} = \begin{bmatrix} q_{11} & q_{12} \\ q_{21} & q_{22} \end{bmatrix} \tag{7}$$

and $\mathbf{b} = [b_1, b_2]^T$. The coefficients of $\mathbf{Q}$ are

$$\begin{aligned} q_{11} &= \sum_i w_i a_{ij}^2 \\ q_{12} = q_{21} &= \sum_i w_i a_{ij} b_{ij} \\ q_{22} &= \sum_i w_i b_{ij}^2. \end{aligned}$$

The two components of $\mathbf{b}$ can be computed directly from the error sinogram $\mathbf{e}$ based on the state of the current voxel $\tilde{x}_j$ such that

$$e_i = y_i - a_{ij}\tilde{\alpha}_j - b_{ij}\tilde{\beta}_j - C_{i,j}.$$

Let's introduce the intermediate vector $\theta_j = [\theta_1, \theta_2]^T$ with

$$\begin{aligned} \theta_1 &= \sum_i w_i e_i a_{ij} \\ \theta_2 &= \sum_i w_i e_i b_{ij}. \end{aligned}$$

Then

$$\mathbf{b} = \theta_j + \mathbf{Q}x_j. \tag{8}$$

Armed with the formulation of equation (6) supported by (7) and (8), the joint optimization of (α_j, β_j) follows the normal rules of standard quadratic framework. For edge-preserving regularization, however, the efficient handling of the non-quadratic prior term in the update equations requires the functional substitution methodology introduced in [7], with implied modifications to $\mathbf{Q}$, θ_1, and θ_2 to take into account the coefficients of the prior model estimated around the current point on the cost function curve.

III. Results

We apply this approach on a scan of a patient's head acquired on a GE LightSpeed CT750 HD scanner obtained from an axial 32x0.625mm protocol. The acquisition is tilted by 16 degrees relative to the table axis in order to minimize radiation dose to the eyes. However this has the consequence of increasing density gradients between bone and soft tissue in the trans-axial reconstruction direction. Figure 3 show the magnitude of the density gradients relative to both the slice before and the slice after the image of interest. The largest magnitude regions are located around the sinuses at the base of the skull where the brain turns into high density bone.

These locations correspond to the areas of partial volume artifacts in the top image of Figure 1. Reconstruction slice thickness equal to the detector row size is standard practice for analytical methods, but is sub-optimal compared to the 0.3125mm sampling dictated by Nyquist for higher quality,

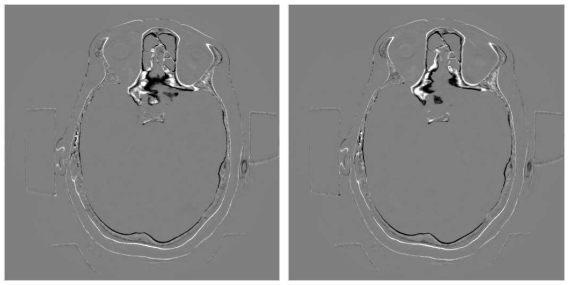

Fig. 3. Density gradients relative to the slice before (left) and after (right) for the image of interest reconstructed in 0.625mm thickness from a patient's axial head scan. The stronger gradients in the trans-axial direction occur around the sinuses at the base of the skull.

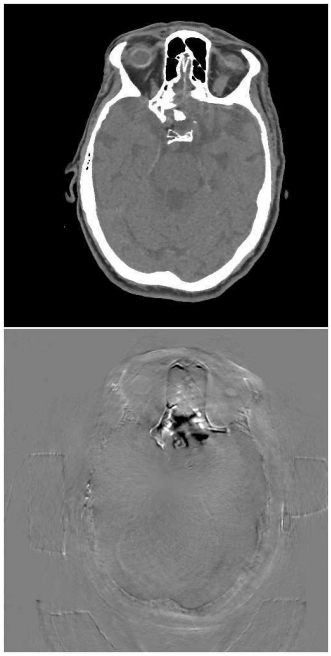

Fig. 4. Top: Piecewise linear iterative reconstruction of the same data as in Figure 1 in 0.625mm image thickness. The linear partial volume artifact around the sinus area has been resolved. Bottom: Slope coefficient for the slice above. As expected, the slope coefficient remains near zero except in those areas of strong longitudinal gradient.

as illustrated with the bottom image of Figure 1. To retain the computational advantages of estimating the volume with 0.625mm voxels, we apply the linear parametric model of section II in the longitudinal direction, which better represents the strong gradients in the object. The joint three-dimensional reconstruction is initialized with FBP images for the DC image component, and the first order local gradient computed from these FBP images for the slope coefficient. The result in Figure 4 shows that the partial volume issue has been successfully eliminated. The quality of this image compares favorably to the 0.3125mm reconstruction achieved at higher computation cost.

Fig. 5. Residual error sinogram after convergence down to 1HU of average change to the image volume of Figures 1 and 4 for the standard 0.625mm constant voxel reconstruction (top), the thin slice 0.3125mm constant voxel reconstruction (middle), and the 0.625mm piecewise linear iterative reconstruction (bottom). The magnitude of the residual error is clearly reduced when using the piecewise linear model.

Interestingly, it is also apparent from the residual error sinogram plots in Figure 5 that the piecewise linear model results in a better outcome. Once convergence has been achieved, the residual is mostly comprised of model mismatch error. That is, the remaining error includes the features of the acquired data that cannot be explained well by the reconstruction model. In this case, the choice of 0.625mm piecewise constant longitudinal voxels does not explain well the gradients in the data, and the residual error contains structures of relatively large magnitude in the top image of Figure 5. Those structures are significantly reduced in the residual error of both the 0.3125mm constant voxel model and the 0.625mm piecewise linear models at the middle and bottom of Figure 5. Although some structured error still remains because the models are not strictly representative of reality, one might argue that the piecewise linear model corresponds to the better description of all three models.

In spite of double the number of unknowns, convergence down to less than 1 HU change over the reconstructed volume was achieved in the same number of iterations for all models. NH-ICD was conditioned by the DC image component updates for each voxel to control the voxel selection process. Overall computation was only increased by 15% for a straightforward implementation of the algorithm running on an Intel Nehalem platform. This contrasts with significantly longer reconstruction for the 0.3125mm grid. Significant potential for optimization remains. In particular, the extra computation for the slope component can be done only in parts of the volume with strong gradients by simple thresholding. As illustrated in Figure 4, the image of the slope coefficient remains near zero in all regions with small gradient magnitude along z and could be ignored. This would significantly speed up the execution as regions affected by partial volume are limited to a very small number of voxels compared to the full volume. This kind of flexibility is well supported by the sequential voxel-based approach of ICD. It would be more difficult for global update methods to capitalize on this potential optimization.

IV. Conclusion

We have proposed a framework for parametric modeling of the reconstructed image volume to address issues of linear partial volume in regions of strong density gradients at reduced computational cost. Although the method has been illustrated in a one-dimensional context looking at quality as a function of reconstructed slice thickness, this approach can be extended to other dimensions as well for in-plane improvements. Whereas image pixel size is sufficiently small relative to CT detector angular sampling for most practical targeted situations, full field of view reconstructions on small grids have been found to emphasize aliasing in some situations. This could be addressed using piecewise linear or higher order image models, similarly to the model proposed in this paper.

References

[1] J.-B. Thibault, K. D. Sauer, C. A. Bouman, and J. Hsieh, "A three-dimensional statistical approach to improved image quality for multislice helical CT," *Medical Physics*, vol. 34, no. 11, pp. 4526–4544, 2007. [Online]. Available: http://link.aip.org/link/?MPH/34/4526/1

[2] D. Marin, R. Nelson, and et al., "Detection of hypervascular liver tumors in mdct: Optimization of tube potential for radiation dose reduction and image quality improvement using a model-based iterative reconstruction algorithm," in *Proc. of the RSNA Annual Meeting*, Nov. 2010.

[3] A. Ziegler, T. Koehler, T. Nielsen, and R. Proksa, "Iterative cone-beam CT image reconstruction with spherically symmetric basis functions," in *Proc. Intl. Conf. on Fully 3D Reconstruction in Radiology and Nuclear Medicine*, Salt Lake City, UT, July 6-9 2005, pp. 80–83.

[4] B. DeMan and S. Basu, "Distance-driven projection and backprojection: extension to three dimensions and analysis," *Physics in Medicine & Biology*, vol. 49, pp. 2463–2475, 2004.

[5] Z. Yu, J.-B. Thibault, C. Bouman, K. Sauer, and J. Hsieh, "Fast model-based x-ray CT reconstruction using spatially non-homogeneous ICD optimization," *IEEE Trans. in Img. Proc.*, vol. 20, no. 1, pp. 161–175, Jan. 2011.

[6] M. Kamasak, C. Bouman, E. Morris, and K. Sauer, "Direct reconstruction of kinetic parameter images from dynamic PET data," *IEEE Trans. in Medical Imaging*, vol. 24, no. 5, pp. 636–650, May 2005.

[7] Z. Yu, J.-B. Thibault, K. Sauer, C. Bouman, and J. Hsieh, "Accelerated line search for coordinate descent optimization," in *Proc. of Medical Imaging Conf.*, vol. 6498, no. 41, San Jose, CA, Oct 29 - Nov 4 2006, pp. 2841–2844.